

IMPROVED SPECTRAL LINE TREATMENT AND STELLAR  
ATMOSPHERIC MODELLING FOR CHROMASTARPY

by

Jason H.T. Bayer

A THESIS SUBMITTED IN PARTIAL FULFILMENT OF  
THE REQUIREMENTS FOR THE DEGREE OF

BACHELOR OF SCIENCE

in

Honours Astrophysics

(Department of Astronomy and Physics, Dr. Ian C. Short supervising faculty)

.....  
.....  
.....  
.....  
.....

SAINT MARY'S UNIVERSITY

March 31, 2019

© Jason H.T. Bayer, 2019

## ABSTRACT

ChromaStarPy is a stellar atmosphere and spectrum modeling code written in python designed to give good approximations of stellar spectra, whilst being easily accessible to students at a wide range of levels. We present several projects including: 1) Incorporating a more accurate interpolation of temperature-dependent partition functions; 2) Fitting more realistic limb darkening curves to surface intensity distributions; and 3) Using a new model atom treatment for spectral lines. The new limb darkening curves are based on least-square fitting of linear and quadratic limb darkening laws to the surface intensity distribution separately at each wavelength, and for the Johnson-Bessel filters. In doing so more accurate limb darkening coefficients (LDCs) are produced. The improved partition function treatment is based on fitting a cubic interpolation function to the variation with temperature and produces smooth variations of number densities of elements in each ionization stage with depth. The new model atom treatment allows us to improve the treatment of natural line broadening, producing line profiles that are closer to the observed line width.

---

IMPROVED SPECTRAL LINE TREATMENT AND STELLAR ATMOSPHERIC  
MODELLING

by *Jason H.T. Bayer*

submitted on March 31, 2019:

# Contents

<b>Contents</b> . . . . .	iv
<b>List of Figures</b> . . . . .	vi
<b>List of Tables</b> . . . . .	vii
<b>1 INTRODUCTION</b> . . . . .	1
1.1 STELLAR CLASSIFICATION AND PHOTOMETRY . . . . .	2
1.2 SPECTRAL LINES . . . . .	3
1.2.1 CURVES OF GROWTH AND ELEMENTAL ABUNDANCE . . . . .	3
1.2.2 LINE BROADENING MECHANISMS . . . . .	4
1.3 ENERGY LEVEL STRUCTURE AND PARTITION FUNCTIONS . . . . .	6
1.3.1 ATOMIC ENERGY LEVELS AND IONIZATION . . . . .	6
1.3.2 PARTITION FUNCTIONS AND THE SAHA EQUATION . . . . .	6
1.4 Limb Darkening Curves (LDCs) . . . . .	7
<b>2 Methodology</b> . . . . .	9
2.1 LDC Fitting . . . . .	9
2.2 Partition Function Interpolation . . . . .	11
2.3 Incorporation of Model Atom Data . . . . .	12



---

<b>3 Results</b> . . . . .	15
3.1 Limb Darkening Curve Fits . . . . .	15
3.1.1 Solar Model Limb Darkening Curves . . . . .	15
3.1.2 Arcturus Model Limb Darkening Curves . . . . .	19
3.2 Ionization Fractions and Partition Functions . . . . .	22
3.3 Natural Broadening . . . . .	27
3.3.1 Solar Model Ca II Triplet Lines . . . . .	27
3.3.2 Arcturus Model Ca II Triplet Lines . . . . .	30
3.4 Conclusion . . . . .	32
<b>A Name of your first Appendix</b> . . . . .	34
<b>Bibliography</b> . . . . .	35

---

# List of Figures

1.1	Limb Darkening Visualization . . . . .	8
3.1	Monochromatic Limb Darkening Plot (Sun) . . . . .	17
3.2	Johnson-Bessel Limb Darkening Curves (Sun) . . . . .	18
3.3	Monochromatic Limb Darkening Plot (Arcturus) . . . . .	20
3.4	Johnson-Bessel Limb Darkening Curves (Arcturus) . . . . .	21
3.5	Li I Partition Function . . . . .	23
3.6	C I Partition Function . . . . .	24
3.7	$\frac{N_{II}}{N_I}$ Metal Fraction (Sun) . . . . .	25
3.8	$\frac{N_{III}}{N_{II}}$ Metal Fraction (Sun) . . . . .	26
3.9	Ca II 849.80 nm Line (Sun) . . . . .	28
3.10	Ca II 854.21 nm Line (Sun) . . . . .	29
3.11	Ca II 866.21 nm Line (Sun) . . . . .	29
3.12	Ca II 849.80 nm Line (Arcturus) . . . . .	30
3.13	Ca II 854.21 nm Line (Arcturus) . . . . .	31
3.14	Ca II 866.21 nm Line (Arcturus) . . . . .	31

# List of Tables

3.1	Monochromatic LDC values for linear (columns 2-3) and quadratic (columns 4 - 6) limb darkening laws. Column 1: $\lambda$ value. Columns 2 and 4: $R^2$ values as defined by Equation 2.1. Columns 3, 5, and 6: LDC values. . . . .	17
3.2	Same as Table 3.1 except band-integrated $I(\theta)$ values are through the Johnson-Bessel filters with band center $\lambda_0$ (Column 1) . . . . .	18
3.3	Same as Table 3.1. . . . .	20
3.4	Same as Table 3.2. . . . .	21

# Chapter 1

## INTRODUCTION

The stellar atmosphere is an important structure of stars, as it is the only region of a star that is observable. This is the region between the interstellar medium (ISM), and the stellar interior (Gray, 1992). A star radiates nearly as a blackbody showing a dark line spectrum, as it is surrounded by the atmosphere containing various chemical species that give rise to their own spectral absorption lines. The overall pattern of a line is dependent on three basic parameters: effective temperature,  $T_{\text{eff}}$ , metallicity, a ratio of other elements to hydrogen,  $[\frac{M}{H}]$ , and surface gravity,  $\log(g)$ . Spectroscopy and photometry are often used to determine these parameters. Bandpass photometry is used to construct color-magnitude diagrams of stellar populations to probe the changes associated with stellar evolution (Gray, 1992).

It is also useful to run simulations so an observer can predict or verify observations. This process involves computing a stellar atmosphere using  $T_{\text{eff}}$ ,  $[\frac{M}{H}]$ , and  $\log(g)$  to compute other various properties such as pressure,  $P(r)$ , and temperature,  $T(r)$ , as functions of depth (Gray, 1992). Structures such as  $P(r)$  and  $T(r)$  are calculated by finding solutions to energy conservation, hydrostatic equilibrium, and energy transport equations, in addition to the equation of state (EOS) for the simulated stellar gas and radiation field (See Ch.9. of Gray (1992)). After this an intensity spec-

trum,  $I_\lambda(\theta)$ , emerging from the surface is computed using the modelled atmospheric structure and input elemental abundances that determined the spectral line profiles.

## 1.1 STELLAR CLASSIFICATION AND PHOTOMETRY

It was sought to categorize stars based on what lines were present in their spectra, and hence the MK system as developed. Both  $T_{\text{eff}}$  and bolometric luminosity,  $L_{\text{bol}}$ , can be correlated to a given spectral class. The MK system consists of seven classes in order of decreasing temperature: O, B, A, F, G, K, and M, with subclasses of decreasing  $T_{\text{eff}}$  on integer or half values from zero to nine. The 11 most common luminosity classes in decreasing order of  $L_{\text{bol}}$  are: 0, I, Ia, Ib, II-III, IIIa, IIIab, IIIb, III-IV, and V (Gray, 1992). Both classes together are considered a spectral type. It is often useful to measure the brightness of a star through photometric bands that allow only specific wavelength ranges to be recorded on a detector, the most common of which being the Johnson-Bessel UBVRI filters. A magnitude measured through a filter,  $m_{\text{filter}}$ , can be calculated via:

$$m_{\text{filter}} = -2.5 \log \int_0^\infty F_\nu W_{\text{filter}}(\nu) d\nu + C \quad (1.1)$$

where  $F_\nu$  is the monochromatic flux at  $d\nu$  weighted by the spectral window  $W_{\text{filter}}(\nu)$  and  $C$  is a constant to normalize the magnitude such that an A0 V star would have an appropriate value in that band (Gray, 1992). A color is a difference in magnitude

of an object between two bands, for example:

$$m_B - m_V = -2.5 \log \frac{\int_0^\infty F_\nu W_B(\nu) d\nu}{\int_0^\infty F_\nu W_V(\nu) d\nu} + 0.0710 \quad (1.2)$$

(Gray, 1992).

## 1.2 SPECTRAL LINES

### 1.2.1 CURVES OF GROWTH AND ELEMENTAL ABUNDANCE

Spectral lines arise from atomic transitions between lower energy states,  $E_i$ , and higher energy states,  $E_j$ . The line is centered around a wavelength,  $\lambda_0$ , being inversely proportional to the difference in upper and lower energy levels by  $\Delta E = E_j - E_i = \frac{hc}{\lambda_0}$  where  $h$  is plank's constant and  $c$  is the speed of light. Curves-of-growth (COGs) allow for consistency between spectrographs, and an expression of line strength in units of wavelength (Rutten, 2003). A COG is a plot of equivalent width,  $W_\lambda(N_a)$ , the normalized area of a spectral line under the flux curve,  $F_\lambda$ , with respect to the local continuum flux,  $F_\lambda^c$ , and be described by the equation:

$$W_\lambda(N_a) = \int_{\lambda_1}^{\lambda_2} \frac{F_\lambda^c - F_\lambda}{F_\lambda^c} d\lambda \quad (1.3)$$

where  $\lambda_1$  and  $\lambda_2$  are the limits of integration that define the region of interest of a spectrum (Carroll and Ostile, 2007). The  $W_\lambda(N_a)$  curve has three regimes that correspond to different line strengths proportional to  $N_a$  for weak lines,  $\sqrt{\ln(N_a)}$  for

strong lines, and  $\sqrt{N_a}$  for saturated lines (Carroll and Ostile, 2007). COGs allow for us to determine the number of absorbing atoms contributing to a spectral line's strength, especially for weak lines where a COG is most sensitive.

## 1.2.2 LINE BROADENING MECHANISMS

### NATURAL BROADENING

Natural broadening is a result of the energy time uncertainty principle, namely:

$$\Delta t \Delta E_j \geq \frac{h}{2\pi} \quad (1.4)$$

where  $\Delta t$  is the average lifetime in the upper energy level,  $\Delta E_j$  is the uncertainty in energy of the upper level of a transition, and  $h$  is plank's constant. This causes a spectral line to have a contribution to width of  $\Delta\lambda$  inversely proportional to  $\Delta E_j$  (Carroll and Ostile, 2007).

### THERMAL BROADENING

In a gas, particles have randomly distributed velocities which correspond to a doppler shift in wavelength,  $\Delta\lambda$ , given by:

$$\frac{\Delta\lambda}{\lambda_0} = \frac{v_r}{c} \quad (1.5)$$

where  $\lambda_0$  is the center line wavelength of an atomic transition,  $c$  is the speed of light, and  $v_r$  is the velocity in the direction of observer (Gray, 1992). Taking the average

---

velocity,  $v_0$ , to be  $(\frac{2kT}{m})^{1/2}$ , where  $m$  is the mass of the particle,  $T$  is the temperature of the gas and  $k$  is the Boltzmann constant,  $\Delta\lambda$  can be written as:

$$\Delta\lambda = \frac{\lambda}{c} \left( \frac{2kT}{m} \right)^{1/2} \quad (1.6)$$

(Gray, 1992).

### ZEEMAN EFFECT

In the presence of a magnetic field of strength  $B$ , a particle can have degenerate quantum states for a principle quantum number,  $n$ . For each set of quantum states defined by  $n$  there is  $2j + 1$  states, where  $j$  is the sum of the spin,  $s$ , and angular momentum,  $l$ , quantum numbers (Griffiths, 2005). With more allowed energies there are more transitions allowed with a greater range of wavelengths for the spectral line causing broadening.

### PRESSURE BROADENING

In a gas where particles interactions are frequent, energy levels can become perturbed, and lines broaden. This affect is difficult to model, but has similar affects to natural broadening. The amount of broadening due to these perturbations is approximated by:

$$\Delta\lambda = \frac{\lambda^2 n_0 \sigma}{c\pi} \left( \frac{2kT}{m} \right)^{1/2} \quad (1.7)$$

where  $n_0$  is the number density of the gas,  $\sigma$  is the collisional cross section and the other variables are described in the Thermal Broadening Section (Carroll and Ostile,



2007).

## 1.3 ENERGY LEVEL STRUCTURE AND PARTITION FUNCTIONS

### 1.3.1 ATOMIC ENERGY LEVELS AND IONIZATION

Each electron in an atom is described by its own quantum state, and hence quantum numbers, the most important of which being the principle quantum number  $n$ . The value of  $n$  describes which of the many possible discretized energies the electron has (Gray, 1992). An electron can become excited to higher energy states when it interacts with other particles, typically a photon (Gray, 1992). In these higher states the electron is unstable with a preference of occupying the ground state (having the lowest possible bound-state energy), so shortly after excitation an electron will move to a lower energy state and release a photon with energy  $\Delta E$  and center line wavelength  $\lambda_0$  (Carroll and Ostile, 2007). If an electron gains too much energy it may become unbound from its nucleus (ionized), becoming a free particle.

### 1.3.2 PARTITION FUNCTIONS AND THE SAHA EQUATION

In order to determine the strength of spectral lines, we need to know the number density of particles for each species,  $N_a$ . For a gas dominated by collisions, the distribution of chemical elements over their ionization stages can be expressed by the

Saha equation:

$$\frac{N_{i+1}}{N_i} = \frac{2(2\pi m)^{3/2}(kT)^{5/2}}{P_e h^3} \frac{U_{i+1}(T)}{U_i(T)} e^{-\frac{I}{kT}} \quad (1.8)$$

where  $\frac{N_{i+1}}{N_i}$  is the ratio of the density of two successive ionization stages,  $\frac{U_{i+1}(T)}{U_i(T)}$  is the ratio of associated temperature dependent partition functions,  $m$  is electron mass,  $I$  is the lowest ionization potential of the two species,  $P_e$  is the pressure from the free electrons, and all other variables are as describing the Section 1.1 (Carroll and Ostile, 2007). A partition function can be given by the formula:

$$U_m(T) = \sum_m g_m e^{-\chi_m/kT} \quad (1.9)$$

where  $g_m$  is equal to  $2J + 1$  where  $J$  is the inner quantum of the  $m^{th}$  state and  $\chi_m$  is the energy of the  $m^{th}$  state (Gray, 1992). It is often difficult to calculate this sum for any given temperature and hence partition functions are rarely calculated in detail every time they are needed (Gray, 1992). It will be seen later in Section 2.2 that one way to help mitigate this is by calculating a partition function for a few temperatures and interpolating the rest.

## 1.4 Limb Darkening Curves (LDCs)

Limb darkening is an observable affect where the intensity,  $I_\lambda(\theta)$ , decreases from the center,  $\theta = 0$ , to the limb,  $\theta = 90^\circ$  (See Figure 1.1). After a monochromatic intensity distribution is modelled, a limb darkening law can then be fit to this distribution

usually via a linear function:

$$\frac{I_\lambda(\theta)}{I_\lambda(0)} = 1 - \epsilon_1(\lambda)(1 - \cos\theta) \quad (1.10)$$

or quadratic:

$$\frac{I_\lambda(\theta)}{I_\lambda(0)} = 1 - \epsilon_1(\lambda)(1 - \cos\theta) - \epsilon_2(\lambda)(1 - \cos\theta)^2 \quad (1.11)$$

where  $\epsilon_1(\lambda)$  and  $\epsilon_2(\lambda)$  are the linear and quadratic monochromatic limb darkening coefficients respectively (Claret and Bloemen, 2011). These models become useful when examining eclipsing binary systems and line-of-sight transiting exoplanets as they change the amount of flux reaching a detector.

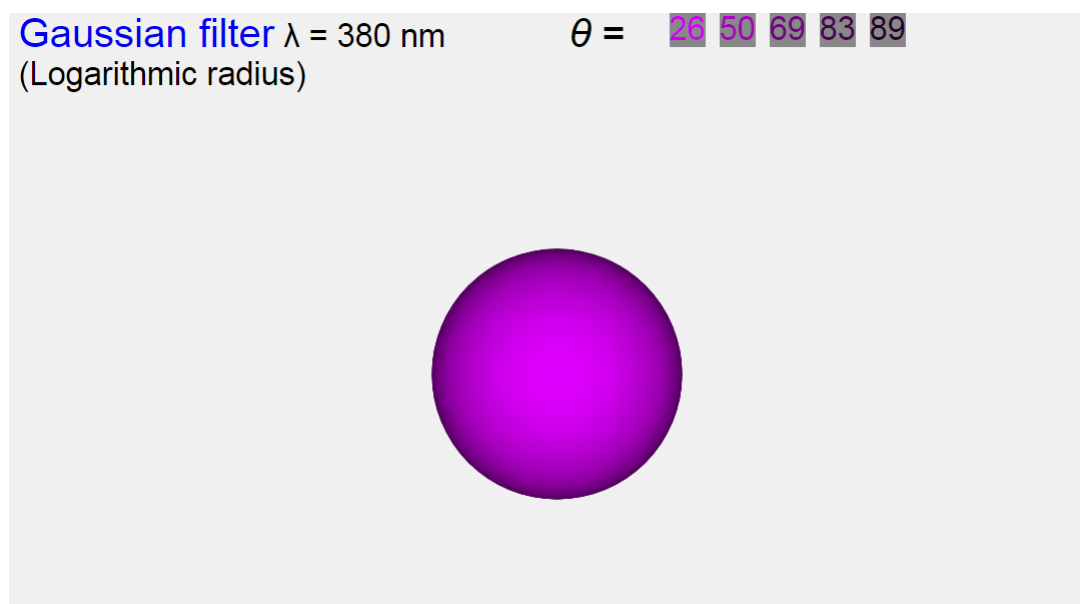


Figure 1.1: Limb darkening of the Sun through a Gaussian filter centered at 380nm and width 0.1nm (computed using ChromaStar: <http://www.ap.smu.ca/ishort/OpenStars/ChromaStar/ChromaStar.html>).

# Chapter 2

## Methodology

### 2.1 LDC Fitting

The source file `LDC.py` holds functions that determine  $\epsilon$  values for a wavelength grid, `lambdaScale`, and for the Johnson-Bessel U, B, B<sub>x</sub>, V, R, I, H, J, K filters. All of these functions return an array of  $\epsilon$  sorted by either increasing wavelength,  $\lambda$ , or index associated with a Johnson-Bessel filter that is determined by the input array holding filter intensities,  $I_{\text{filter}}(\theta)$ , `bandIntens`. The LDCs in Section 3.1 are created using a separate program, from the computed  $\epsilon$  values in the output files created by running the main program `ChromaStarPy.py`.

All functions that determine  $\epsilon$  values for `lambdaScale` have the following input parameters: number of  $\lambda$  values in wavelength grid, `numLams`; the wavelength grid, `lambdaScale`; the number of angles where emergent  $I_{\lambda}(\theta)$  values were calculated, `numThetas`; the cosine of  $\theta$  values with respect to the local surface normal, `cosTheta`; and  $I_{\lambda}(\theta)$  at each  $\theta$  for all  $\lambda$  in the grid, `contIntens`. For functions determining  $\epsilon$  values of the Johnson-Bessel filters,  $\epsilon_{\text{filter}}$ , all parameters are similar except, `numLams` is replaced with `numBands`, the number of bands we are calculating  $\epsilon_{\text{filter}}$  values for, and `contIntens` is replaced with `bandIntens`, which holds  $I_{\text{filter}}(\theta)$  at each  $\theta$  as seen through each band. With these parameters  $I_{\lambda}(\theta)$  in Equations 1.10, and 1.11 or

$I_{\text{filter}}(\theta)$  can be fit with LDCs that best approximate the distribution of intensities.

To get the best  $\epsilon$  for a given  $I_{\lambda}(\theta)$  or  $I_{\text{filter}}(\theta)$  the Python `scipy.curve_fit` fitting method was used. The parameters for `curve_fit` are, the function we are fitting (Equations 1.10 and 1.11) and coordinates for the points we are trying to fit, in this case each point having at  $\frac{I_{\lambda}(\theta)}{I_{\lambda}(0)}$  (or  $\frac{I_{\text{filter}}(\theta)}{I_{\text{filter}}(0)}$ ) on the vertical axis and  $\cos(\theta)$  on the horizontal. Non-linear least-squared statistics were used to determine the  $\epsilon$  values that give the best  $R^2$  value ( $R_L^2$  for  $\epsilon_1$  and  $R_Q^2$  for  $\epsilon_2$ ), which is given by:

$$R^2 = 1 - \frac{\Delta y_r}{\Delta y} \quad (2.1)$$

where  $\Delta y_r$  is the summed residuals and  $\Delta y$  is the variance of  $\frac{I_{\lambda}(\theta)}{I_{\lambda}(0)}$ . If  $R^2 = 1$  then the model is a perfect fit for  $\frac{I_{\lambda}(\theta)}{I_{\lambda}(0)}$ . The  $\epsilon$  that gives an  $R^2$  closest to one is stored as the  $\epsilon$  for that band or  $\lambda$ . Residuals are determined by the expression:

$$\Delta y_r = \sum_{k=0}^N (y_k - f_k)^2 \quad (2.2)$$

where  $k$  is the index of the `cosTheta` and `contIntens` (or `bandIntens`) arrays,  $N$  is `numThetas`,  $y_k$  is  $\frac{I_{\lambda}(\theta)}{I_{\lambda}(0)}$  for a given  $\cos(\theta)$ , and  $f_k$  is the modelled functional value at  $\cos(\theta)$ . The variance is given by the standard formula:

$$\Delta y = \sum_{k=0}^N (y_k - \bar{y})^2 \quad (2.3)$$

where  $\bar{y}$  is the mean of the  $\frac{I_{\lambda}(\theta)}{I_{\lambda}(0)}$  values. After determining the  $\epsilon$  values for each band and  $\lambda$ , the `contIntens`, `bandIntens`, and corresponding  $\epsilon$  arrays are sent to a separate

---

file that uses the Python numpy package to plot the  $\frac{I_\lambda(\theta)}{I_\lambda(0)}$  (or  $\frac{I_{\text{filter}}(\theta)}{I_{\text{filter}}(0)}$ ) with  $\epsilon$  values given by Equations 1.10 and 1.11.

## 2.2 Partition Function Interpolation

ChromaStarPy uses three procedures to calculate opacity,  $\kappa$ , for different chemical species,  $i$ , at 48 optical depths,  $\tau$ : KappasRayl.py does so for Rayleigh scattering of the neutral elements HI and HeI; KappasMetal.py which does so for bound-free transitions of Cl, MgI, MgII, AlI, SiI, SiII, and FeI; and Kappas.py which deals specifically with  $\kappa$  related to the elements H, and He, from free-free, bound-free transitions, and molecular H, H<sub>2</sub>. Using LevelPopsServer.py the number density of  $i$ ,  $n_i$ , for a given  $\tau$  can be calculated. For KappasRayl.py, KappasMetal.py, and LevelPopsServer.py these processes require knowledge of  $U(T)$  (See Equation 1.8).

Previously ChromaStarPy calculated  $U(T)$  via piece-wise linear interpolation for a set of  $U(T)$  values at five temperature points 130, 500, 3000, 8000, and 10000 K from Barklem and Collet (2016), and now utilizes a cubic fit. The fit was done using the Python numpy.polyfit method, which minimizes a least squares fit statistic, and takes arrays holding  $U(T)$  values as input for the dependent variables and temperatures for the independent variables, ordered by increasing temperature (e.g. the zeroth index of  $U(T)$  corresponds to  $T = 500K$ ). The last polyfit parameter is polynomial order, which for this case was set to three for a cubic fit. The output array of polyfit holds

---

the coefficients  $A$ ,  $B$ ,  $C$ , and  $D$  for a generalized cubic of the form:

$$y = Ax^3 + Bx^2 + Cx + D \quad (2.4)$$

where  $y = U(T)$  and  $x = T$  in this case. After a fit is made and stored for each  $U(T)$ , an array of coefficients and any  $T$  can be used to determine the  $U(T)$  value for any  $\tau(\lambda)$ , which helps to determine both  $\kappa$  and  $\frac{N_{i+1}}{N_i}$ .

## 2.3 Incorporation of Model Atom Data

ChromaStarPy previously used line list data, but now uses both model atom and line list data to compute spectral lines for any chemical species. A line list is frequently used as it is presorted via  $\lambda_0$ , holding a corresponding  $E_i$  value and Einstein coefficient for a deexcitation between  $E_i$  and  $E_j$ ,  $A_{ij}$ , among other relevant quantities to computing spectral lines. Model atom data has the same information but is organized such that transitions from  $E_j$  for a given species are easily accounted for, but has to be sorted by  $\lambda_0$  after the value is computed. Once all lines from the line list are read,  $E_i$ ,  $E_j$ ,  $A_{ij}$  and other relevant information to compute spectral lines from Hauschildt et al. (1999) are read in as binary model atom data. The species specified to be treated as a model atom is skipped in the line list as to not compute a spectral line more than once.

The value of  $A_{ij}$  is used to compute  $\gamma_R$ , the radiative dampening constant for the transition, can be determined by summing the Einstein coefficients of downward

transitions from  $E_i$  and  $E_j$ . The relationship between  $\gamma_R$  and  $E_j$  is more explicit for model atom data as compared to the line list as it does not require the sorting of an entire line list via species to compute. The value of  $\gamma_R$  hence can now be computed accurately as a result via the equation:

$$\gamma_R = \sum_{k=0}^{N_{jk}} A_{jk} + \sum_{k=0}^{N_{ik}} A_{ik}, \text{ where } \begin{cases} k < j \forall j \\ k < i \forall i \end{cases} \quad (2.5)$$

and  $N_{jk}$ ,  $N_{ik}$  are the number of transitions downward from  $j$  and  $i$  respectively. The value  $\gamma_R$  is also the inverse of  $\Delta t$  described in Section 1.2.2 and hence is used to determine the amount of natural broadening in the line. The shape of weak, strong, and saturated spectral lines is described by the Voigt function:

$$\psi(\lambda - \lambda_0) = \frac{\lambda_0^2}{c\sqrt{\pi}(\lambda - \lambda_0)} \frac{a}{\pi} \int_{-\infty}^{\infty} \frac{e^{y^2}}{(v - y)^2 + a^2} dy \quad (2.6)$$

where:

$$y = \frac{\zeta \lambda_0}{c \Delta \lambda},$$

$$\zeta = \frac{(\lambda - \lambda_0)}{\lambda_0},$$

$$v = \frac{(\lambda - \lambda_0)}{\Delta \lambda},$$

$$a = \frac{\gamma \lambda_0^2}{\Delta \lambda 4 \pi c},$$

and,

$$\gamma = \gamma_R + \gamma_C$$



where  $\gamma_C$  is the collisional damping constant, and all other variables are described in Section 1 (Rutten, 2003).

# Chapter 3

## Results

### 3.1 Limb Darkening Curve Fits

The Sun and Arcturus are the two chosen test stars for examining limb darkening. The Sun is the most well studied and understood G2 V star, while Arcturus (HR 5340, HD 124897, HIP 69673,  $\alpha$  Boo) is a standard K2 III (red giant) and is the fourth brightest star in the sky with an absolute magnitude,  $M_V$ , of -0.31, an apparent magnitude,  $m_V$ , of -0.05, and from Carroll and Ostile (2007), a color,  $B - V$ , of 0.9 (Prieto and Ramirez, 2011). The Sun by comparison has  $m_V = -26.7$ , and from Carroll and Ostile (2007),  $M_V = 4.82$  and  $B - V = 0.65$  (Engelke et al., 2011). Limb darkening generally is most prominent and linear with respect to  $\cos(\theta)$  in the ultraviolet (UV) becoming non-linear in the infrared (IR). This is a result of the general shape of blackbody, having larger variations in  $\frac{I(\theta)}{I(0)}$  at smaller  $\lambda$ .

#### 3.1.1 Solar Model Limb Darkening Curves

Limb darkening curve fitting for the Sun producing best fit LDC values,  $\epsilon$ , and associated  $R^2$  statistics for linear,  $R_L^2$ , and quadratic  $R_Q^2$  fits. This was done for both representative  $\lambda$  values and the Johnson-Bessel bands which are represented in Tables 3.1 and 3.2. These fits used the following stellar parameters:  $T_{eff} = 5777K$ ,  $[\frac{A}{H}] = 0.0$ ,

---

and  $\log(g) = 4.44$  (Grevesse et al., 1992). The  $\lambda$  values from `lambdaScale` were chosen to accurately represent limb darkening at UV, visible, and IR wavelengths. The  $R^2$  statistics (See Equations 2.1, 2.2) in Tables 3.1, 3.2 are a measure of how well a model with a computed set of  $\epsilon$  fit the distribution of  $\frac{I(\theta)}{I(0)}$ . For the  $\lambda$  values it can be seen that both linear and quadratic models are a better fit than previous method in the IR and visible, whereas only the linear fit shows improvement in the UV. For the chosen set of  $\lambda$ , the visible and IR values are best fit by quadratic limb darkening curves while the linear fit is best for UV as expected. Table 3.2 holds similar information to Table 3.1 but for the Johnson bands with central band wavelength  $\lambda_0$ . In Figure 3.2 a similar trend can be seen, where quadratic fits better describe bands with  $\lambda_0$  in the visible and shorter  $\lambda_0$  IR bands, while bands closest to the UV are best represented by linear fits. Longer IR bands begin to show less variation in  $\frac{I(\theta)}{I(0)}$ , and hence are more linear as shown.

Table 3.1: Monochromatic LDC values for linear (columns 2-3) and quadratic (columns 4 - 6) limb darkening laws. Column 1:  $\lambda$  value. Columns 2 and 4:  $R^2$  values as defined by Equation 2.1. Columns 3, 5, and 6: LDC values.

$\lambda$ [nm]	$R_L^2$	$\epsilon_1$	$R_Q^2$	$\epsilon_1$	$\epsilon_2$
352.35 (UV)	0.9984	0.8308	0.8398	0.02402	0.8108
653.09 (Visible)	0.9524	0.4651	0.9804	0.3007	0.2148
997.64 (IR)	0.9293	0.3343	0.9451	0.2726	0.1075

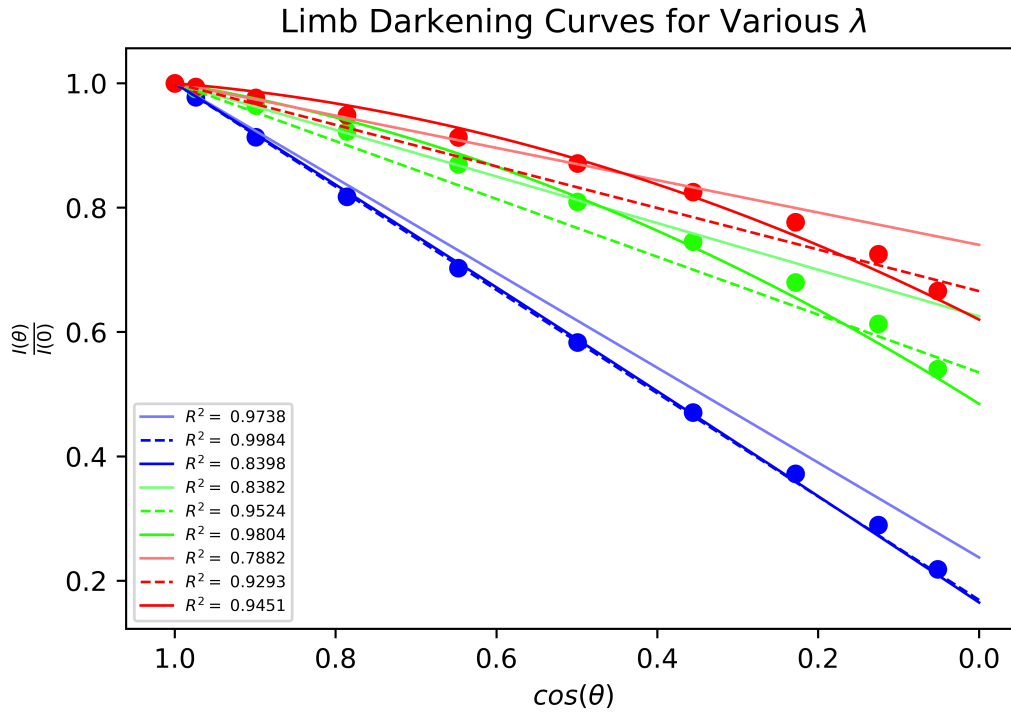


Figure 3.1: Monochromatic limb darkening for 352 (blue), 653 (green), and 997 (red) [nm]. New best fit linear, quadratic, and old limb darkening laws (dashed, dark, and light lines respectively). Dots: Computed  $\frac{I(\theta)}{I(0)}$  values from ChromaStarPy.

Table 3.2: Same as Table 3.1 except band-integrated  $I(\theta)$  values are through the Johnson-Bessel filters with band center  $\lambda_0$  (Column 1)

Band: $\lambda_0$ [nm]	$R_L^2$	$\epsilon_1$	$R_Q^2$	$\epsilon_1$	$\epsilon_2$
$U_x$ : 365	0.9979	0.8142	0.8556	0.0440	0.7776
$B_x$ : 445	0.9875	0.6795	0.9598	0.1988	0.5141
B: 445	0.9879	0.6824	0.9584	0.1963	0.5191
V: 551	0.9687	0.5509	0.9893	0.2796	0.3181
R: 658	0.9545	0.4726	0.9826	0.2974	0.2251
I: 806	0.9378	0.3900	0.9606	0.2940	0.1455
J: 1230	0.9310	0.3118	0.9462	0.2556	0.0991
H: 1630	0.9132	0.2885	0.8953	0.2859	0.0507
K: 2190	0.9043	0.2169	0.8785	0.2217	0.0324

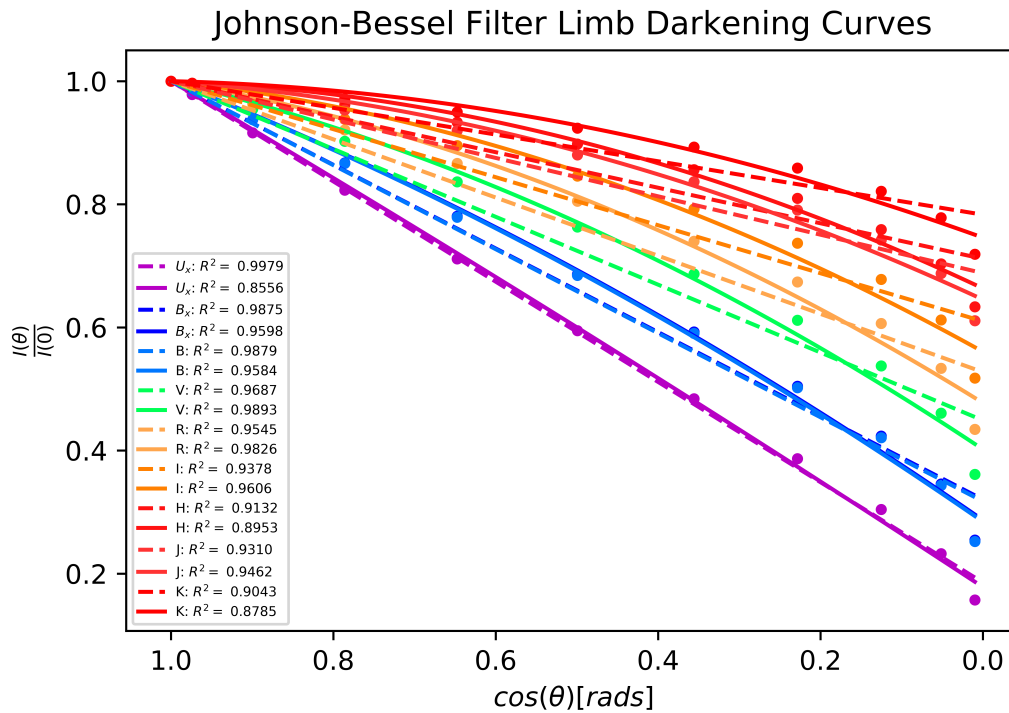


Figure 3.2: Same as Fig. 3.1 except band-integrated  $I(\theta)$  values are through the Johnson-Bessel filters. The colored dots are computed  $\frac{I(\theta)}{I(0)}$  values from ChromaStarPy color-coded according to the plot legend.

---

### 3.1.2 Arcturus Model Limb Darkening Curves

The same statistics and fitting procedures were done for the K star Arcturus using the parameters:  $T_{eff} = 4300$  K,  $[\frac{A}{H}] = -0.7$ , and  $\log(g) = 2.0$  (Griffin and Lynas-Gray, 1999). The same trend for UV, visible, and IR bands are seen as in Section 3.1.1. Visible  $\lambda$  and  $\lambda_0$  values still seem to be best fit by quadratic limb darkening for values  $> 500$ [nm], and the old method of fitting for  $\lambda$  tends to be the same for UV  $\lambda$  but worse than linear fitting otherwise. Quadratic limb darkening tends to be a worse fit for the UV, and longer IR  $\lambda$  and  $\lambda_0$  values when compared to a linear fit.

Table 3.3: Same as Table 3.1.

$\lambda$ [nm]	$R_L^2$	$\epsilon_1$	$R_Q^2$	$\epsilon_1$	$\epsilon_2$
352.35 (UV)	0.9895	0.9791	0.5260	-0.2997	1.2284
653.09 (Visible)	0.9896	0.5868	0.9686	0.3001	0.3370
997.64 (IR)	0.9405	0.4237	0.9640	0.3158	0.1610

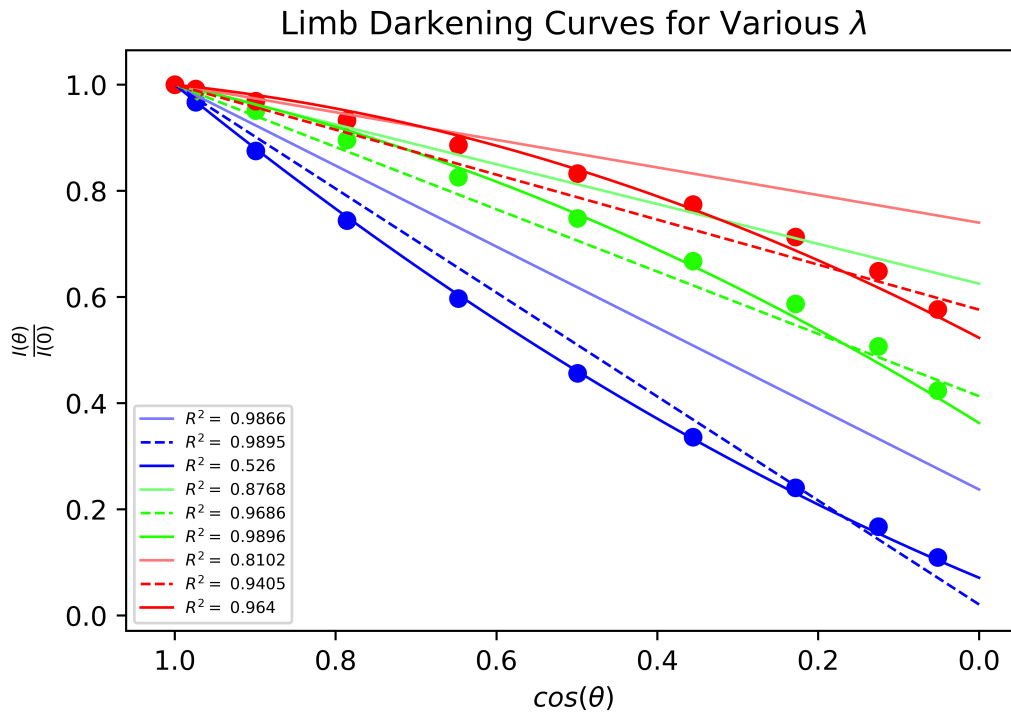
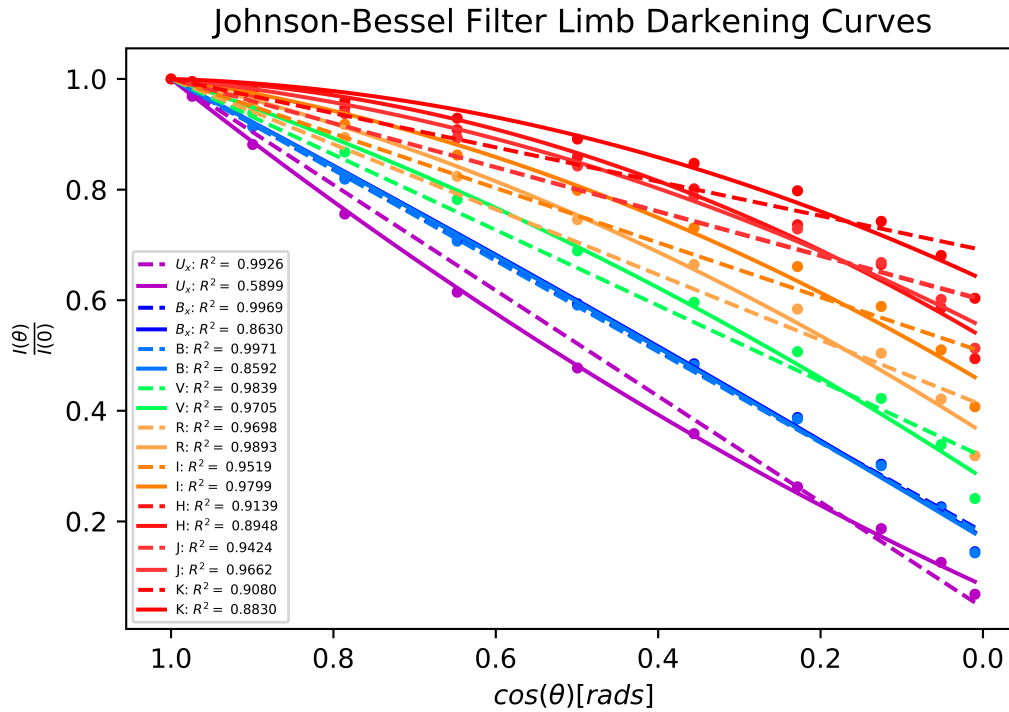


Figure 3.3: Same as Figure 3.1.

Table 3.4: Same as Table 3.2.

Band: $\lambda_0$ [nm]	$R_L^2$	$\epsilon_1$	$R_Q^2$	$\epsilon_1$	$\epsilon_2$
$U_x$ : 365	0.9926	0.9561	0.5899	-0.2408	1.1564
$B_x$ : 445	0.9960	0.8190	0.8630	0.0560	0.7724
B: 445	0.9971	0.8220	0.8592	0.0509	0.7797
V: 551	0.9839	0.6830	0.9705	0.2312	0.4906
R: 658	0.9698	0.5900	0.9893	0.2940	0.3454
I: 806	0.9519	0.4934	0.9799	0.3240	0.2238
J: 1230	0.9424	0.4000	0.9662	0.3983	0.0686
H: 1630	0.9139	0.3989	0.8948	0.2959	0.1525
K: 2190	0.9080	0.3095	0.8830	0.3154	0.0471





## 3.2 Ionization Fractions and Partition Functions

Figures 3.5 and 3.6 show the difference between linear piece-wise (old) and cubic (new) fits for Li I and C I partition function values,  $U(T)$ . In Figure 3.5 it can be seen that cubic fits better represents the five  $U(T)$  values from Barklem and Collet (2016). In Figure 3.6 it can be seen that although the cubic polynomial does not fit the  $U(T)$  values exactly, but allows for more variation between values. Figure 3.7 shows the relative difference of the ionization fractions computed with new and old  $U(T)$  fits between singly-ionized and neutral elements. Again a solar model using the parameters described in Section 3.1.1 was used. To examine the effect of our models it was best to use some of the most abundant metals in the Sun, which includes Ca, Na, K, Fe, Al, Si and Mg. All elements show a relative difference greater than zero for most temperatures, with the greatest difference of 23% deep in the Sun's atmosphere ( $T > 10000$  [K]), which is significant. This is also seen in Figure 3.8 which shows the relative difference between doubly-ionized and singly-ionized elements. The results indicate that our cubic partition functions affect the number density of elements in successive ionization stages as expected.

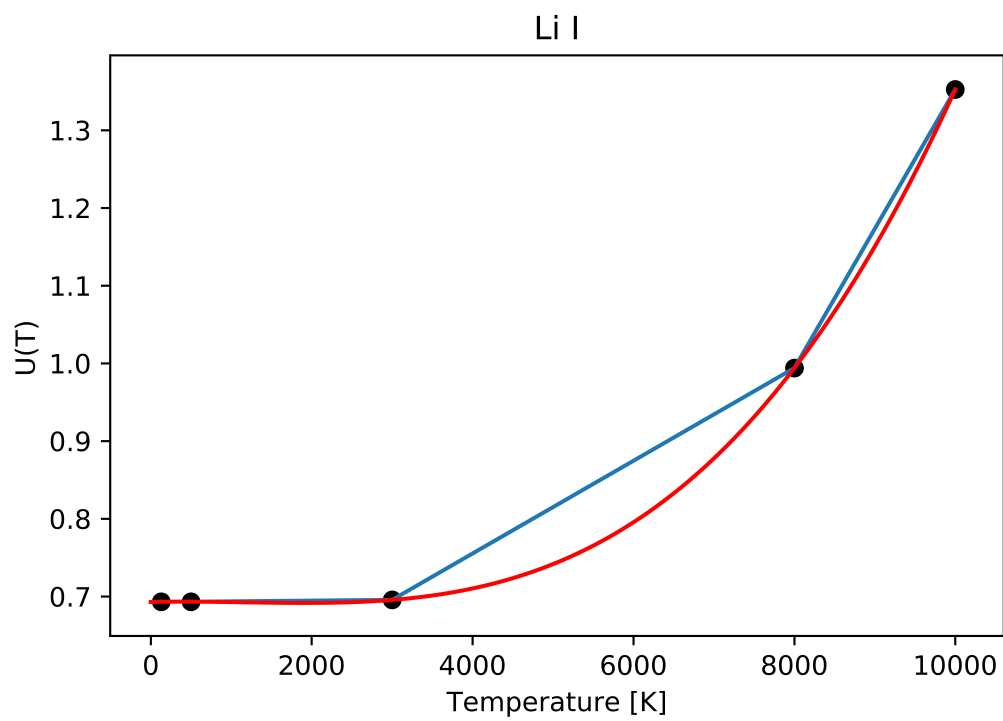


Figure 3.5: A plot of fitted  $U(T)$  values for Li I including linear piece-wise (blue) and cubic (red) fits. The black dots are the published  $U(T)$  values from Barklem and Collet (2016).

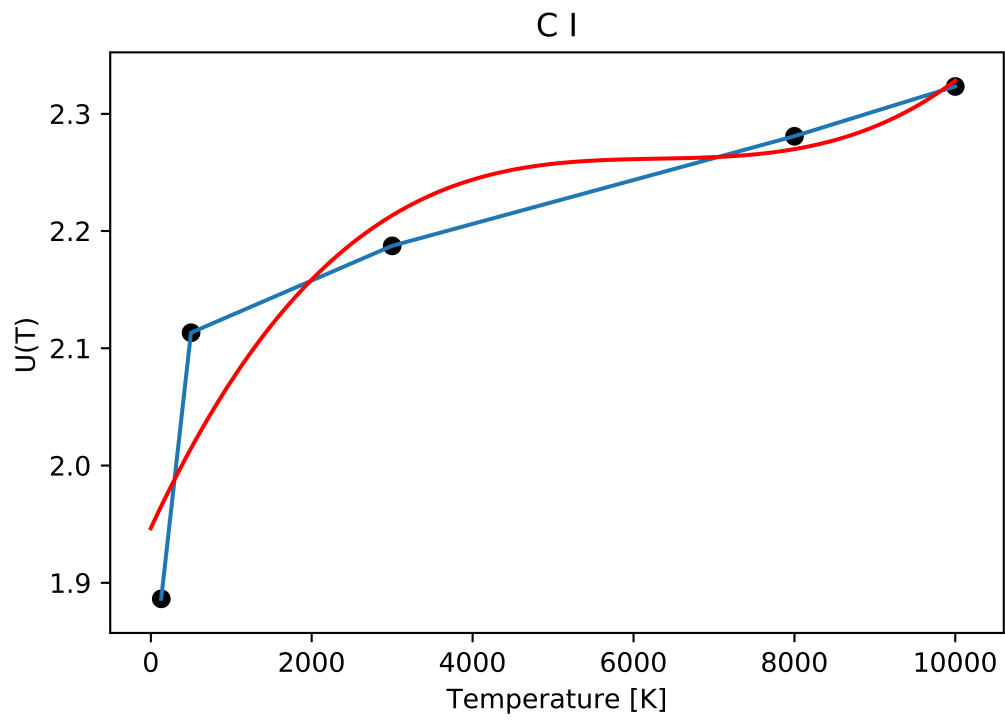


Figure 3.6: Same as Figure 3.5 except for C I.

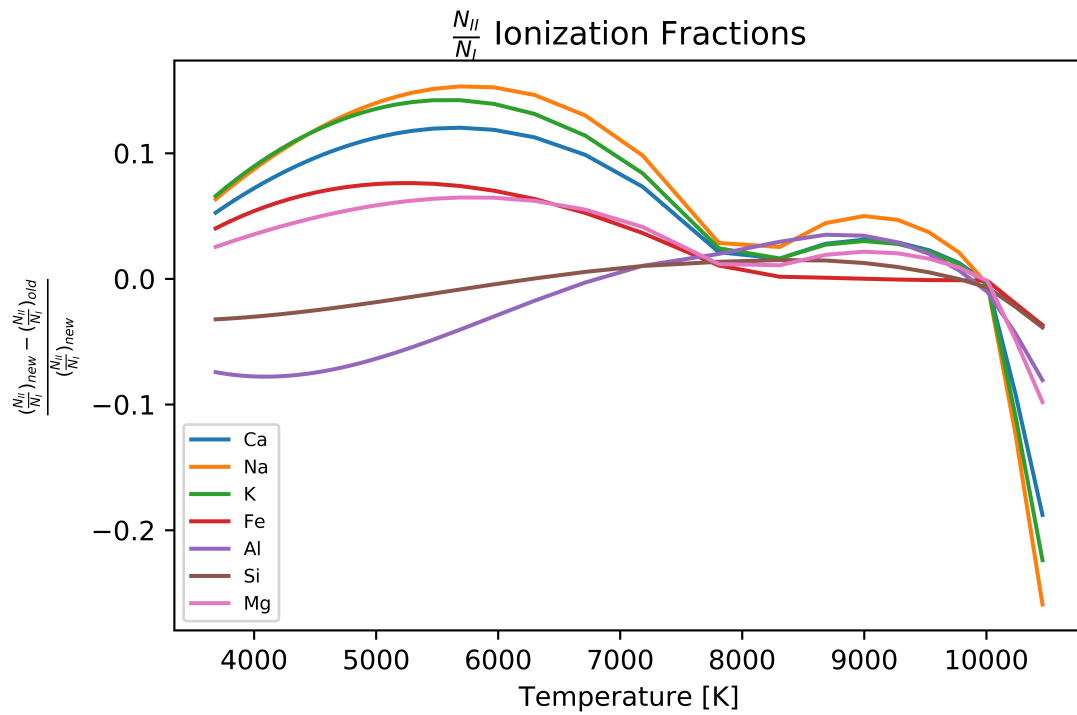


Figure 3.7: Relative difference between the ionization fractions of singly-ionized and neutral species computed with new and old  $U(T)$  fits (See Section 3.2).

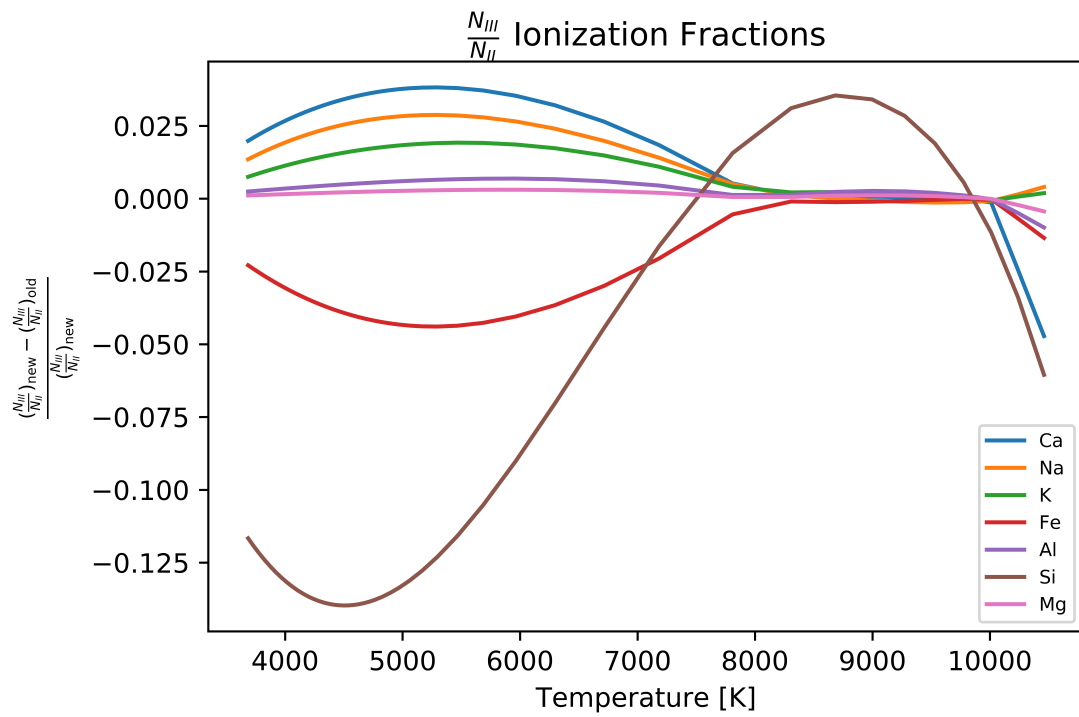


Figure 3.8: Same as Figure 3.7 but for a ratio of doubly-ionized and singly-ionized species.

### 3.3 Natural Broadening

Figures 3.9 - 3.14 show an observed spectrum and two synthetic spectra computed with and without the improved treatment of natural broadening, and the relative difference between the synthetic spectra. As a test case, the Ca II Triplet, a group of lines in the IR band, were chosen as they arise from an upper energy level with a small  $\Delta t$ , hence will be greatly affected by natural broadening (See Section 1.2.2). These lines are particularly prominent in giant (II) stars such as Arcturus, and comparing these lines to the Sun is a good test as pressure broadening is more dominant in dwarf (V) stars. This implies that the line profile will be more sensitive to the improved natural broadening treatment in giants as compared to dwarfs (See Section 3.1 for each star's parameters). It must be noted that generally computed spectral lines are less broad than observed lines as it is difficult to account for all processes contributing to line width. This is consistent throughout Figures 3.9 - 3.14.

#### 3.3.1 Solar Model Ca II Triplet Lines

Figures 3.9 - 3.11 show the three Ca II singlet lines that are part of the Ca II Triplet for the Sun. In the wings of Figure 3.9 and 3.11 there is a difference of no more than 2%, while in Figure 3.10 a difference of 3% can be seen. For each singlet this is inconsistent between each wing, hence indicating that natural broadening contributed minimally to spectral line width. Towards line center larger variations are seen but they are not important when examining broadening.

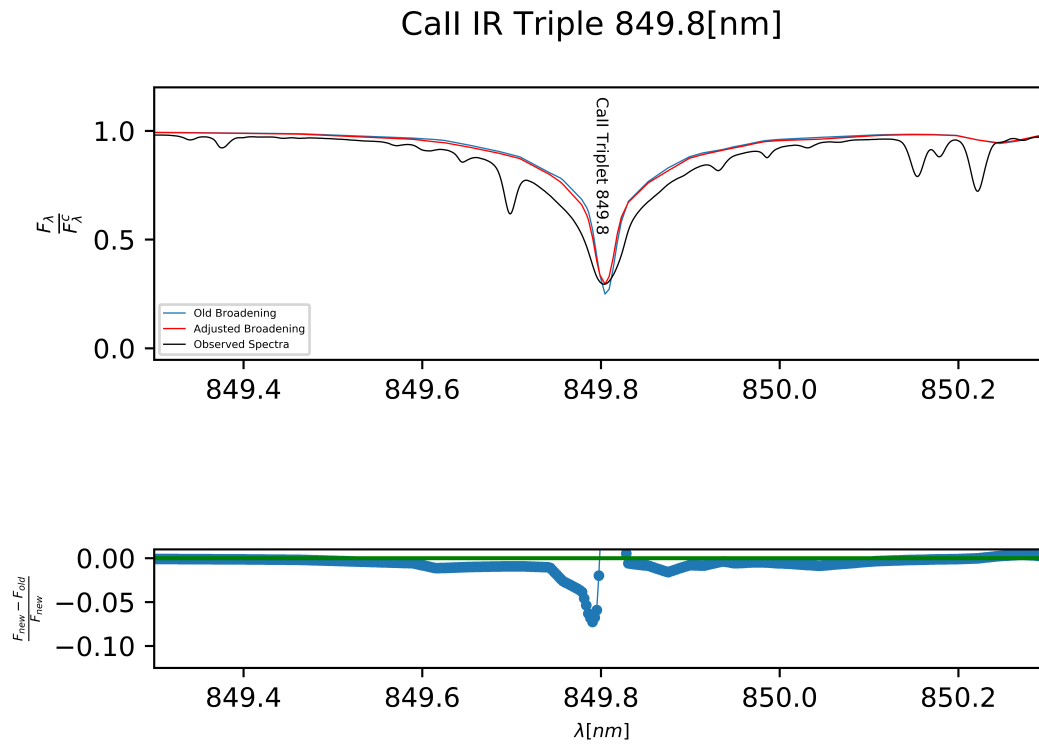


Figure 3.9: Ca II 849.8 [nm] region in the solar flux spectrum. The upper plot shows continuum normalized observed (black line), and synthetic spectra (colored lines). The lower plot shows the relative difference between synthetic spectra.

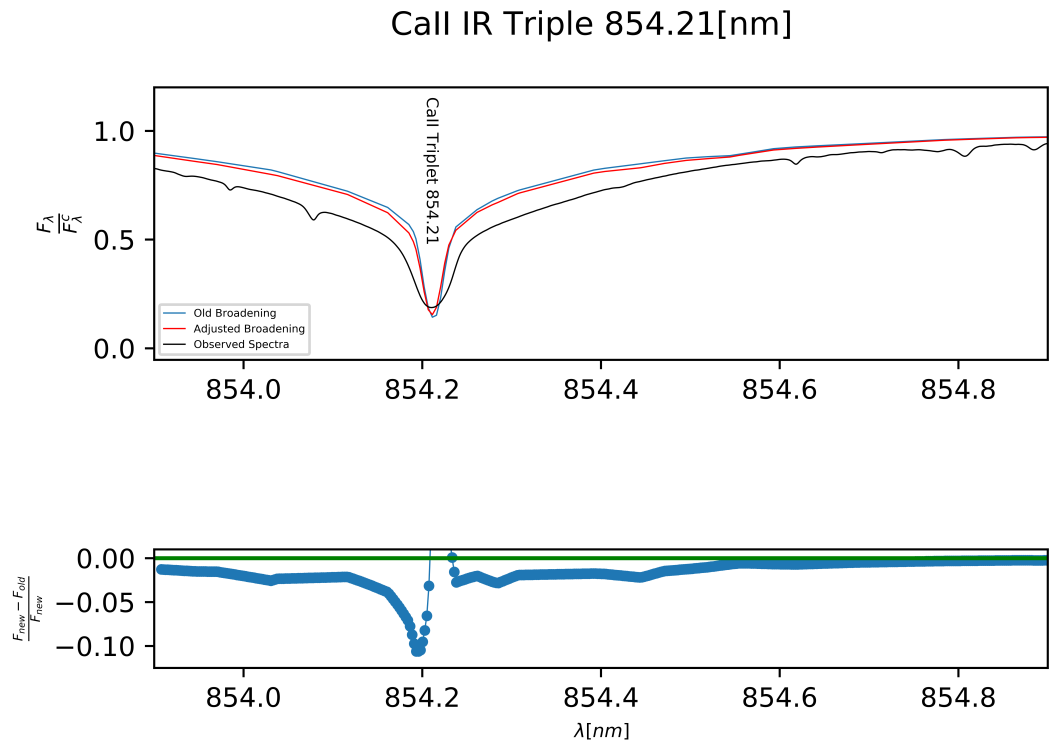


Figure 3.10: Same as Figure 3.9 except for the Ca II 854.21 [nm] region.

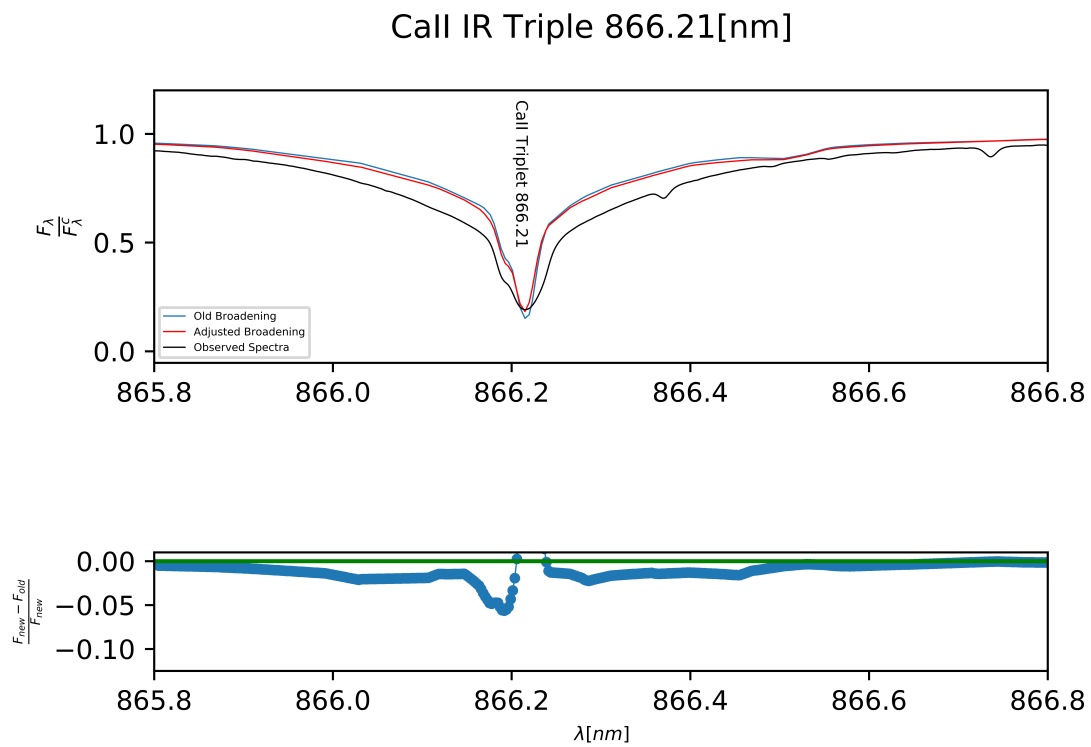


Figure 3.11: Same as Figure 3.9 except for the Ca II 866.21 [nm] region.



### 3.3.2 Arcturus Model Ca II Triplet Lines

Figures 3.12 - 3.14 show the three Ca II singlet lines that are part of the Ca II Triplet for Arcturus. In the wings of Figures 3.12 - 3.14 there is a relative difference between 10 and 15% that is consistently decreasing toward the continuum, where the relative flux between the old and new methods are zero. This is consistent with what would be expected if natural broadening were contributing to line width over other broadening mechanisms.

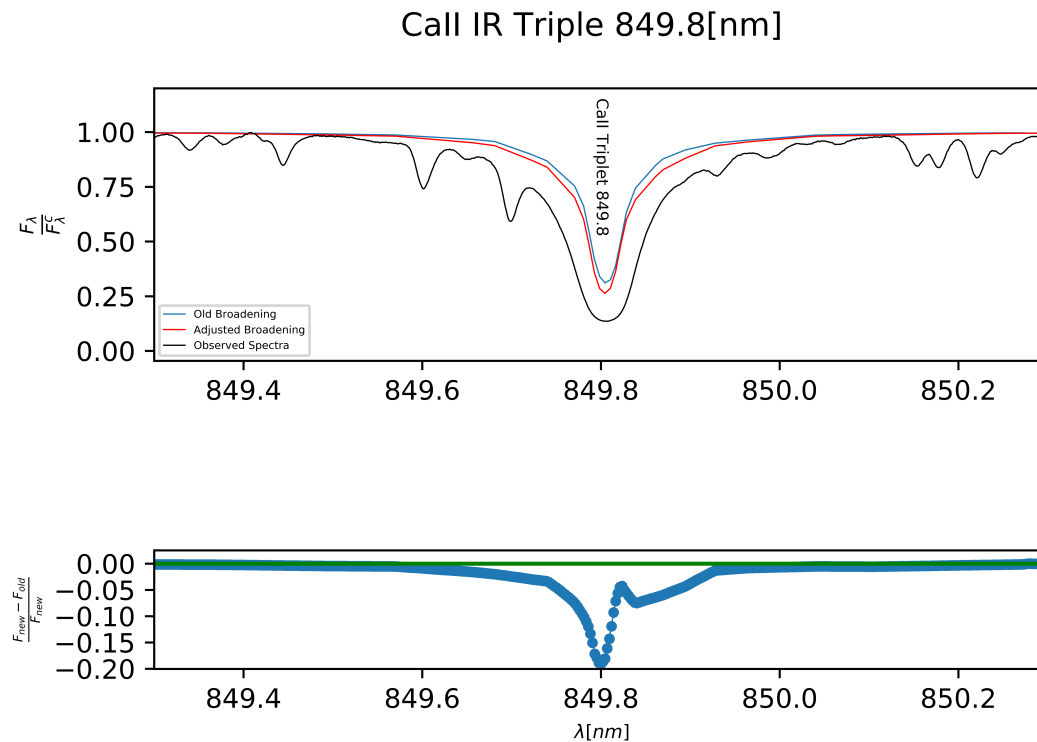


Figure 3.12: Same as Figure 3.9 except for Arcturus.

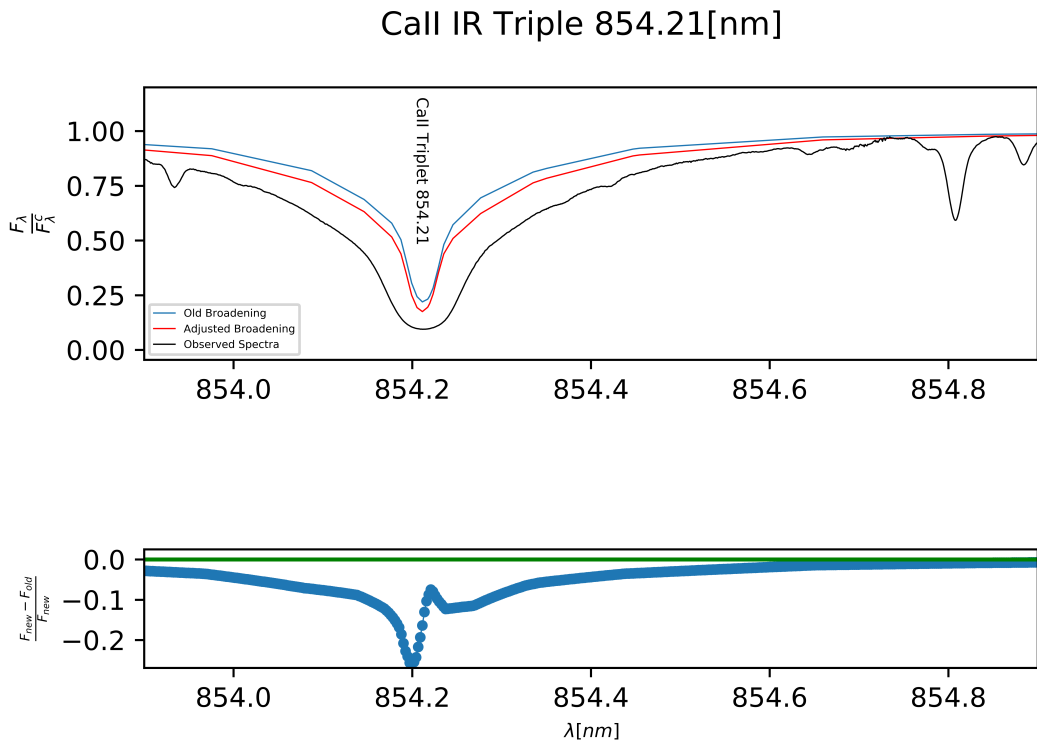


Figure 3.13: Same as Figure 3.12 except for the Ca II 854.21 [nm] region.

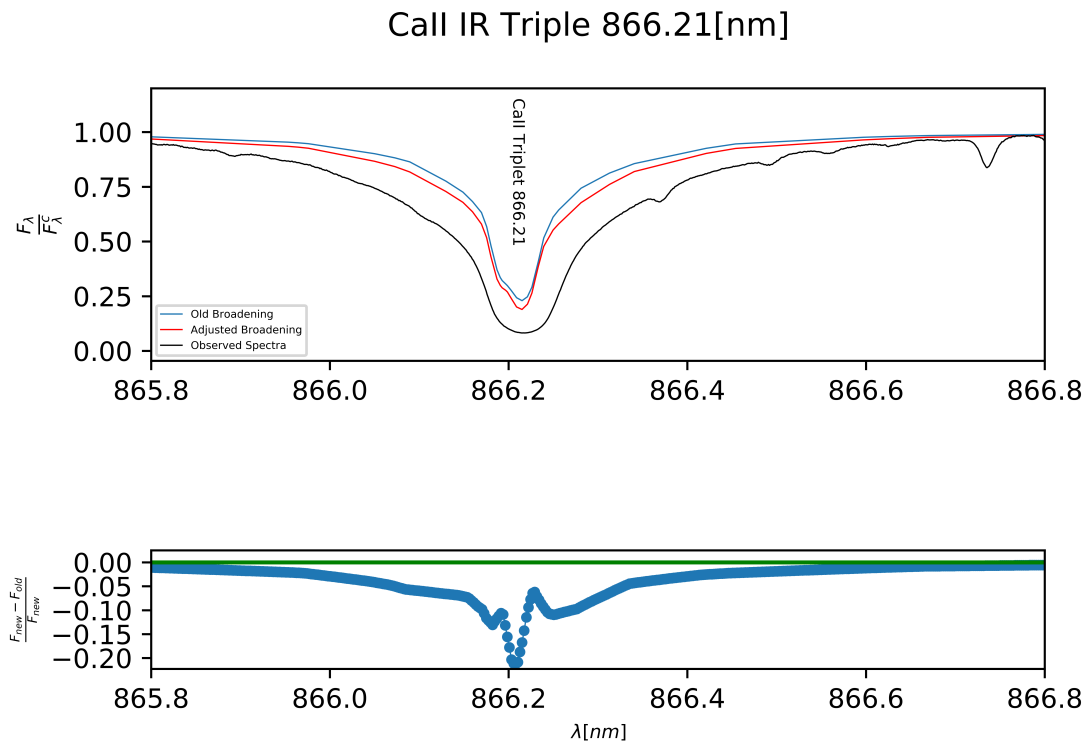


Figure 3.14: Same as Figure 3.12 except for the Ca II 866.21 [nm] region.

# Chapter 4

## Conclusion

ChromaStarPy is a stellar atmosphere and spectrum modelling code designed to be more responsive, and accessible than research grade legacy codes. ChromaStarPy's modelling is approximate, but allows for calculations of potentially observable quantities such as LDC,  $\epsilon$ , values. Throughout this thesis, the code was developed and the effect on predicted observables was studied. This was done for three separate projects including: incorporating a more accurate interpolation of temperature-dependent partition functions; fitting more realistic limb darkening curves to surface intensity distributions; and using a new model atom treatment for spectral lines.

A least-square fitting procedure for linear and quadratic limb darkening laws was fit to the monochromatic intensities,  $\frac{I(\theta)}{I(0)}$ , for monochromatic  $\lambda$  values and band-integrated intensities for the Johnson-Bessel filters with center band wavelength  $\lambda_0$ . The previous fitting method only fit a linear limb darkening law which was done by solving for  $\epsilon$  values in Equation 1.10 and averaging for all  $\theta$  values. Monochromatic  $\lambda$  and  $\lambda_0$  ultraviolet, UV, filters showed either a similar or better fit when compared to the previous method. Monochromatic  $\lambda$  values and bands with  $\lambda_0$  in the shorter infrared, IR, are best fit by quadratic  $\epsilon$  values, and linear  $\epsilon$  values better fit longer IR  $\lambda_0$  bands. Generally the UV and far IR exhibit linear darkening, while intermediate

---

values are better fit by a quadratic limb darkening law. Overall the limb darkening fits behave as such for both the Sun and Arcturus, and linear fits show an either a better or similar fit.

Additionally, the new cubic interpolation of partition functions,  $U(T)$ , better fits published  $U(T)$  values from Barklem and Collet (2016), showing that the new interpolation is an improvement. The new  $U(T)$  values were shown to influence the ionization fractions of the Sun,  $\frac{N_{\text{II}}}{N_{\text{I}}}$  by up to 23% and  $\frac{N_{\text{III}}}{N_{\text{II}}}$  by up to 14%. This difference would be significant enough to influence the metallicity of a star observationally, and is hence significant.

Lastly, the model atom treatment allowed for a more complete calculation of natural line broadening. Comparing the Ca II IR Triplet computed for the Sun and Arcturus proved to be insightful, as these lines are predominantly affected by natural broadening in luminosity class III (giant) stars. For the Sun, a luminosity class V star, no broadening in the spectral wings of the triplet can be seen when using the model atom treatment, which was to be expected as V stars are dominated by pressure broadening. Arcturus, a luminosity class III star, showed a relative difference between the line list and new model atom treatment of 10 to 15%. This analysis showed that the new model atom treatment provided a more accurate calculation of natural line broadening.

---

# Bibliography

P. S. Barklem and R. Collet. *Astronomy & Astrophysics*, 588, 2016.

Bradley W. Carroll and Dale A. Ostlie. *An Introduction to Modern Astrophysics*. Pearson Education Inc., 1301 Sansome Street, San Francisco, CA, USA, 2nd edition, 2007.

A. Claret and S. Bloemen. Gravity and limb-darkening coefficients kepler, corot, spitzer, uvby, ubvrihjk, and sloan photometric systems. *Astronomy & Astrophysics*, 2011.

Charles W. Engelke, Kathleen E. Kraemer, and Stephan D. Price. Spectral irradiance calibration in the infrared. xvii. zero-magnitude broadband flux reference for visible-to-infrared photometry. *The Astrophysical Journal*, 140, 2011.

David F. Gray. *The observation and analysis of stellar photospheres*. Cambridge University Press, 40 West 20th Street, New York, NY, USA, 2nd edition, 1992.

N. Grevesse, A. Noelsand, and A.J. Sauval. Proceedings of the first soho workshop. *ESA*, page 305, 1992.

R. E. M. Griffin and A. E. Lynas-Gray. Proceedings of the first soho workshop. *Astronomical Journal*, 117:305, 1999.

David J. Griffiths. *Introduction To Quantum Mechanics*. Pearson Education, Inc., Upper Saddle River, NJ, USA, 2nd edition, 2005.

P. H. Hauschildt, F. Allard, J. Ferguson, E. Baron, and D. R. Alexander. Proceedings of the first soho workshop. *Astronomical Journal*, 525, 1999.

C. Allende Prieto and I. Ramirez. Fundamental parameters and chemical composition of arcturus. *The Astrophysical Journal*, 743, 2011.

R. J. Rutten. *Radiative Transfer in Stellar Atmospheres*. Sterrekundig Instituut Utrecht, 8th edition, May 2003.